Journal of Nuclear Medicine, published on December 4, 2014 as doi:10.2967/jnumed.114.146944

In Vivo SPECT Imaging of Amyloid-β Deposition with Radioiodinated Imidazo[1,2-*a*]pyridine Derivative DRM106 in Mouse Model of Alzheimer's Disease

Chun-Jen Chen[1, 2, 3], Kazunori Bando[1], Hiroki Ashino[1], Kazumi Taguchi[1], Hideaki Shiraishi[1], Keiji Shima[1], Osuke Fujimoto[1], Chiemi Kitamura[1], Satoshi Matsushima[1], Keisuke Uchida[1], Yuto Nakahara[1], Hiroyuki Kasahara[1], Takao Minamizawa[1], Cheng Jiang[4], Ming-Rong Zhang[2], Maiko Ono[2], Masaki Tokunaga[2], Tetsuya Suhara[2], Makoto Higuchi[2], Kazutaka Yamada[3] and Bin Ji[2, *]

[1] Research Department, Fujifilm RI Pharma Co. LTD, Chiba, Japan

[2] Molecular Imaging Center, National Institute of Radiological Sciences, Chiba, Japan

[3] Clinical Veterinary Science, The United Graduate School of Veterinary Science, Gifu University, Gifu, Japan

[4] School of Pharmacy, Fudan University, Shanghai, China

* Corresponding author: Bin Ji, Ph.D.

Molecular Imaging Center, National Institute of Radiological Sciences, 4-9-1, Anagawa, Inage-ku, Chiba-shi, Chiba 263-8555, Japan, Phone: +81-43-206-3251. Fax:

+81-43-253-0396. E-mail: kihin@nirs.go.jp

First author: Chun-Jen Chen, Fellow.

Fujifilm RI Pharma Co. LTD, Chiba, Japan, 453-1, Shimo-Okura, Matsuo-Machi, Sammu-Shi, Chiba, 289-1592, Japan, Phone: +81-479-86-4722. Fax: +81-479-86-3522. E-mail: chchusei@ffri.co.jp

Word count: 4940

Short running head: Amyloid SPECT with DRM106

This work was supported in part by Grants-in-Aid for Japan Advanced Molecular Imaging Program and Core Research for Evolutional Science and Technology (T. S.) and Scientific Research on Innovative Areas ("Brain Environment") 23111009 (M. H.) from the Ministry of Education, Culture, Sports, Science and Technology, Japan.

ABSTRACT

Non-invasive determination of amyloid-β peptide (Aβ) deposition has important significance for early diagnosis and medical intervention for Alzheimer's disease (AD). In the present study, we investigated the availability of radiolabeled DRM106 ($^{123/125}$I-DRM106), a compound with sufficient affinity for the synthesis of human Aβ fibrils and satisfactory metabolic stability, as a single photon emission computed tomography (SPECT) ligand in living brains. **Method:** The sensitivity of ^{125}I-DRM106 for detecting Aβ deposition was compared with ^{125}I-IMPY, a well-known amyloid SPECT ligand, by ex vivo autoradiographic analyses in 18-month-old amyloid precursor protein transgenic (Tg) mice. To verify the sensitivity and quantitation of radiolabeled DRM106 for in vivo imaging, we compared the detectability of Aβ plaques with ^{123}I-DRM106 and a well-known amyloid positron emission tomography (PET) agent, ^{11}C-labeled Pittsburgh compound B (^{11}C-PiB), in 29-month-old Tg mice and age-matched non-Tg littermates. Additionally, we compared the binding characteristics of ^{125}I-DRM106 with those of ^{11}C-PiB and ^{11}C-PBB3, which selectively bind to Aβ plaques and preferentially to tau aggregates, respectively, in postmortem AD brain sections. **Results:** Ex vivo autoradiographic analysis showed that measurement with ^{125}I-DRM106 has higher

sensitivity for detecting Aβ accumulation than with ^{125}I-IMPY in Tg mice. SPECT imaging with ^{123}I-DRM106 also successfully detected Aβ deposition in living aged Tg mice, and showed strong correlation ($R = 0.95$, $p < 0.01$) in quantitative analysis for Aβ plaque detection by PET imaging with ^{11}C-PiB, implying that sensitivity and quantitation of SPECT imaging with ^{123}I-DRM106 are almost as good as ^{11}C-PiB-PET for the detectability of Aβ deposition. Further, the addition of non-radiolabeled DRM106 fully blocked the binding of ^{125}I-DRM106 and ^{11}C-PiB, but not ^{11}C-PBB3, to AD brain sections, and ^{125}I-DRM106 showed a lower binding ratio of the diffuse plaque-rich lateral temporal cortex to the dense cored/neuritic plaque-rich hippocampal CA1 area, compared to ^{11}C-PiB.

Conclusion: All of these data demonstrated the high potential of ^{123}I-DRM106 for amyloid imaging in preclinical and clinical application, and it might more preferentially detect dense-cored/neuritic amyloid deposition, which is expected to be closely associated with neuropathological changes of AD.

Keywords: Alzheimer's disease (AD); Amyloid imaging; Amyloid precursor protein (APP) transgenic mouse; DRM106; Single photon emission computed tomography (SPECT)

INTRODUCTION

Alzheimer's disease (AD) is a progressive neurodegenerative disorder characterized by two pathological hallmarks of amyloid-β peptide (Aβ) plaques and neurofibrillary tangles. In vivo non-invasive detection of Aβ deposition is important for early diagnosis and medical intervention of AD at a prodromal stage, since fibrillary Aβ has already been accumulating in the brain for a few decades prior to AD onset (*1*). Molecular imaging with nuclear medicine technologies such as positron emission tomography (PET) and single photon emission computed tomography (SPECT) is available for both preclinical and clinical use, and is considered as a bridge between them. Over the past few years, the availabilities of several PET tracers for amyloid imaging have been successfully verified in AD patients. ^{11}C-labeled Pittsburgh compound B (^{11}C-PiB) is a most widely used PET ligand, with which investigators have assessed the longitudinal, quantitative Aβ accumulation in AD model mice and patients (*2-4*), and verified amyloid deposition as a useful imaging biomarker for AD diagnosis, prognostic judgment for conversion from mild cognitive impairment (MCI) to AD, and evaluation for anti-amyloid therapies (*5-7*). To overcome the shortcoming of the limited half-life (approximately 20 min) of ^{11}C-labeled tracers, ligands

labeled with ^{18}F (half-life: approximately 110 min) have also been developed for further routine medical needs (*8-11*).

Although inferior to PET in terms of sensitivity and quantitative performance, single photon emission computed tomography (SPECT) imaging has advantages of operating cost and already-installed rate in medical hospitals, making it more suitable for primary screening for prodromal AD patients. For the past decade, several SPECT ligands have been developed for amyloid imaging. ^{123}I-IMPY is a SPECT tracer with high affinity for Aβ fibrils, and in vitro autoradiographic analysis has successfully detected amyloid deposition on brain sections from both AD models and AD patients (*12-16*). However, preliminary clinical data for ^{123}I-IMPY showed a poor signal-to-noise ratio, making it difficult to distinguish between cognitively normal persons and AD patients, possibly due to insufficient affinity for Aβ fibrils, poor brain permeability or metabolic instability (*17*). Very recently, we developed a series of imidazopyridine compounds for amyloid SPECT imaging, and obtained a promising candidate compound, termed DRM106, which has higher affinity for synthetic human Aβ fibrils and metabolic stability. In vitro autoradiography with ^{125}I-labeled DRM106 also successfully detected Aβ plaques in postmortem AD patient brains (*18*). In the present study, we performed in vivo imaging

with this newly developed SPECT ligand in living model mice with AD-like amyloid pathology, and compared it with ^{11}C-PiB in the detectability of Aβ deposition.

MATERIALS AND METHODS

Radiosynthesis of Radioligands

Radiosynthesis of ^{125}I-DRM106 (6-Iodo-2-[4-(1*H*-3-pyrazolyl)phenyl]imidazo[1,2-*a*]pyridine), ^{125}I-IMPY, ^{11}C-PiB and ^{11}C-PBB3 (2-((1*E*,3*E*)-4-(6-(11C-Methylamino)pyridin-3-yl)buta-1,3-dienyl)benzo[*d*]thiazol-6-ol) was performed as described in previous publications (*2,12,18,19*). The radiochemical purity of ^{125}I-DRM106, ^{125}I-IMPY, ^{11}C-PiB and ^{11}C-PBB3 was > 95%, and specific radioactivity was 81.4, 81.4, 93-354, and 72-204 GBq/μmol, respectively, at the end of synthesis.

^{123}I-DRM106 was prepared by the reaction of its precursor with ^{123}I-NaI in the presence of chloramine T (Fig. 1). Briefly, chloramine T (0.035 mg / 20 μL 2-propanol) was added to 4.5 mL of 35 mM phosphate buffer (pH 6.3) containing ^{123}I-NaI (29.9 GBq; Fujifilm RI

Pharma Co., Ltd (specific activity was adjusted to 714 GBq/μmol by addition of non-radiolabeled NaI)), and precursor (0.638 mg), and incubated for 5 min at room temperature, followed by quenching by the addition of 200 μL of 1 N NaOH. Then, the reaction mixture was incubated at 70°C for 30 min and terminated by cooling. The subsequent experimental procedure was the same, with preparation of ^{125}I-DRM106, as described in our previous publication (*18*). The radiolabelling efficiency of ^{123}I-DRM106 was 65-80% based on radio-TLC measurement. The radiochemical purity was > 95% at the end of synthesis and the theoretical value of the specific activity was 714 GBq/μmol, considering that the reaction of ^{123}I-NaI and precursor led to the formation of ^{123}I-DRM106 with a 1:1 stoichiometric ratio.

Experimental Animals

A transgenic (Tg) mouse line (Tg2576), which overexpresses a mutant form of amyloid precursor protein (APPK670/671L), was purchased from Taconic Farms Inc.. Then, we generated JU-Tg2576 mouse by backcrossing of Tg2576 with JU strain (JU/Ct-C, A.) mouse over 29 generations under license agreement of the Mayo Foundation for Medical Education and Research from Daiichi Sankyo Co. Ltd. for easier daily handling. Tg mice

(termed JU-Tg2576 if without special description) and body weight-matched non-Tg JU strain mice as control animals were used in the present study, except for in vivo SPECT imaging, for which commercially available Tg2576 mouse brain was used.

Preparation of Brain Homogenates and Aβ Fibrils, In Vitro Binding Assay and Aβ Assessment, In Vitro and Ex Vivo Autoradiographic Analysis and Metabolite Analysis, Small Animal PET and SPECT Imaging

Experimental procedures are presented in ***Supplemental Information***.

Statistical Analysis

All statistical examinations in the present study were performed by SPSS software. Statistical analyses for group comparisons were performed by Student's t-test or analysis of variance (ANOVA) followed by Bonferroni's post hoc test. Correlation between two parameters was examined by parametric test with Pearson product-moment correlation coefficient (R). The difference between groups was considered significant at p value < 0.05. All data were expressed as mean ± SD (standard deviation).

RESULTS

In Vitro Binding of DRM106

Saturation curves and Scatchard analyses using a two-site binding model demonstrated that K_d values of high-affinity binding sites of DRM106 to synthetic human Aβ(1-40) and Aβ(1-42) fibrils, brain homogenates of Tg mice and AD patients were approximately 1 to 10 nM, and low-affinity sites were approximately 100 to 300 nM (SFig. 1, Table 1). To estimate the correlation between quantitative ^{125}I-DRM106 binding and Aβ amounts, brain homogenates of Tg mice at different ages (8.1 to 17 months) were used for measurement of ^{125}I-DRM106 binding and Aβ amounts. Age-dependent increases in ^{125}I-DRM106 binding and Aβ amounts were detected, and there was excellent correlation between ^{125}I-DRM106 binding and the amount of either Aβ(1-40) ($R = 1$, $p < 0.01$) or Aβ(1-42) ($R = 0.99$, $p < 0.01$) (Fig. 2).

Metabolite Analysis in Tg mice

Solutions of ^{125}I-DRM106 (1.1 MBq) were injected into male JU-Tg2576 Tg mice (18 months old) via tail vein, and metabolite analyses were performed as described in our

previous publication (*18*). Similar to results in normal rats (*18*), there were no detectable metabolites in the brain over the observation period, while only a little metabolite-related radioactivity was observable in the plasma samples, in addition to unchanged ^{125}I-DRM106 (Fig. 3).

Ex Vivo Autoradiography with ^{125}I-DRM106 and ^{125}I-IMPY

The sensitivity of ^{125}I-DRM106 for detecting Aβ plaques was higher than that of ^{125}I-IMPY, based on the experimental observation that more amyloid plaques were detectable by using ^{125}I-DRM106 than ^{125}I-IMPY at three indicated time points in 18-month-old Tg mice (Fig. 4). Meanwhile, no overt difference in amyloid deposition labeled by congo red was detectable between two experimental groups for ^{125}I-DRM106 and ^{125}I-IMPY analysis (data not shown). Although slight non-specific binding of ^{125}I-DRM106 to white matter was detectable in both Tg and non-Tg mice at 1 h post-injection, background radioactivity decreased to an undetectable level after 2 h (Fig. 4A), suggesting that optimum scan time for in vivo imaging with radiolabeled DRM106 was between 1 and 2 h for acquiring good contrast with minimum loss in radioactive signals. Ex vivo emulsion autoradiography and consequent fluorescent labeling with thioflavin-S showed great consistency of

^{125}I-DRM106 accumulation and thioflavin-S-positive Aβ deposition (SFig. 2).

In Vivo Imaging with ^{123}I-DRM106 SPECT and ^{11}C-PiB PET

To investigate the capacity of ^{123}I-DRM106 for in vivo detection of amyloid deposition, we performed in vivo imaging with ^{123}I-DRM106 and ^{11}C-PiB in the same mice and compared their quantitative analysis. The accumulation of ^{11}C-PiB in the frontal/parietal cortex (CT) and hippocampus (Hip) regions enriched with amyloid deposition was more abundant compared with that in other brain regions in Tg mice (Tg2576), while no regional difference in radioactivity accumulation was detectable in age-matched non-Tg mice. In vivo images of ^{123}I-DRM106 showed great similarity to those of ^{11}C-PiB except for more intelligible accumulation in the cerebellum (CB) (Fig. 5A, SFig. 3). Subsequent ex vivo autoradiography also clearly demonstrated consistency in radioligand accumulation with the observation of in vivo imaging. Quantitative analysis showed that both ^{11}C-PiB and ^{123}I-DRM106 accumulations in amyloid pathology-enriched regions (CT/Hip) in Tg mice were significantly higher than in non-Tg mice (Fig. 5B). Positive correlations between amyloid depositions detected by these two radioligands ($R = 0.95$; $p < 0.01$), and between in vivo and ex vivo binding of ^{123}I-DRM106 ($R = 0.98$; $p < 0.01$) were statistically

significant (Fig. 5C). Although using CB with slight～moderate amyloid pathology as reference tissue would underestimate the binding potential calculated from the simplified reference tissue model, this would not affect our correlation analysis.

Binding of ^{125}I-DRM106, ^{11}C-PiB and ^{11}C-PBB3 in Postmortem Human Brain

To evaluate binding sites of ^{125}I-DRM106 in AD brain, we compared the in vitro autoradiographic images of ^{125}I-DRM106 with ^{11}C-PiB or ^{11}C-PBB3, a radiolabeled ligand that binds to both amyloid and tau lesions at 5 nM of incubation concentration (*19*), in AD brain sections containing the Hip and temporal cortex (TCx) regions. The addition of non-radiolabeled DRM106 fully blocked the binding of ^{125}I-DRM106, ^{11}C-PiB, and partially ^{11}C-PBB3, in AD brain sections (Fig. 6A). All of ^{125}I-DRM106, ^{11}C-PiB, and ^{11}C-PBB3 showed detectable specific binding in TCx regions harboring numerous plaques including dense-cored/neuritic and diffuse plaques and NFTs, and in the hippocampal CA1 sector enriched with NFTs and Aβ deposition composed of numerous dense-cored/neuritic and few diffuse plaques, to greater or lesser degrees (Fig. 6B, C, SFig. 4). The TCx-to-CA1 ratio of DRM106 binding was similar to that of PBB3, but significantly lower than that of PiB (Fig. 6D).

DISCUSSION

For development of SPECT ligand for amyloid imaging, the compound IMPY is a good guide because it is the first SPECT imaging agent to be tested in human subjects, and a lot of data has already been published for reference. In vitro autography with ^{123}I-IMPY clearly demonstrated its availability for visualization of Aβ plaques in either AD model (APP/PS1 double-Tg mouse) or postmortem brain sections. Ex vivo autographic analysis also visually confirmed ^{123}I-IMPY-labeled Aβ plaques in aged APP/PS1 double-Tg mice (*12*). The results of in vivo imaging with microSPECT, however, were not very encouraging (*17*). Subsequent clinical studies also showed that the signal-to-noisy ratio for plaque labeling was not as high as that of ^{11}C-PiB (*17*). This indicates that successful development will require higher criteria as exemplified by higher metabolic stability and affinity for Aβ plaques than IMPY. The present and previous data clearly demonstrated that ^{125}I-DRM106 has satisfactory metabolic stability in rodents and higher affinity for synthetic human Aβ fibrils than IMPY (*18*). There was high-level specific binding of ^{123}I-DRM106 to Aβ deposition in Tg2576 mouse and postmortem AD patient brains with high affinity (K_d of one-digit nM). This characteristic was similar to that of ^{11}C-PiB, as published in a previous study, at low nanomolar concentrations typically used in SPECT studies (*20*). Such

improvements in the properties of imaging agents are responsible for the superiority of ^{125}I-DRM106 in the detectability of Aβ plaques compared to ^{125}I-IMPY, as shown in ex vivo autoradiographic analysis (Fig. 4). Very recently, amyloid deposition in 28-month-old Tg2576 mice was successfully visualized with a radioiodine-labeled pyridyl benzofuran derivative (*21*). There was, however, relatively high retention, approximately 40% of initial brain uptake, in normal brain even after 60 min, and resulting high-level non-specific binding to white matter (*21*). Given that white matter in human subjects is much more abundant than in rodents, such high-level non-specific binding to white matter may overtly affect the detectability of Aβ plaques in human subjects. Additionally, this radioligand was not metabolically stable in normal mouse. The intact form in plasma was decreased to approximately 20% at 30 min post-injection (*21*), raising the undesirable possibility that these radioactive metabolites penetrated into the brain and lowered the signal-to-noise ratio. In contrast, the amount of ^{125}I-DRM106 remaining in normal brain was lowered to less than 4% of initially uptake after 60 min, exhibiting excellent off-target washout (*18*). As a result, there was very low non-specific binding in white matter and other brain regions without amyloid pathology (Figs. 4, 5). Additionally, we have noted a recent poster presentation (Alzheimer Association International Conference 2014, Copenhagen), where a newly

developed radioiodinated tracer, ^{123}I-ABC577, seemed available for image-based diagnosis for AD in human subjects. Although this is a preliminary result and there is still a lack of accurate information available, such as the chemical structure of ABC577, this successful case has proved the feasibility of SPECT agent for amyloid imaging in human subjects.

In comparison with PET, radioisotopes used in SPECT, such as ^{123}I (half-life: 13.22 h), have a longer half-life and can therefore achieve longer distance delivery and cheaper operating cost, and more SPECT scanners have also been installed for routine clinical examinations, making it more suitable for primary screening for prodromal AD patients, especially in developing countries with large territories. Given that the sensitivity and quantitativity of SEPCT are inferior to those of PET, we need more in vivo imaging data to support the availability of DRM106 for further clinical application. We performed in vivo imaging with ^{123}I-DRM106 in Tg2576 mice and compared this with PET imaging with ^{11}C-PiB. Tg2576 is a widely used transgenic mouse line with AD-like amyloid pathology, with Aβ plaque density increasing exponentially from 12 months, reaching levels similar to those seen in AD brain (*22*). There were, however, many fewer amyloid-associated binding sites for ^{11}C-PiB in Tg2576 mouse, compared to AD patient tissues (*2,23*). Despite the fewer binding sites for ^{11}C-PiB in Tg2576 mouse, we successfully detected significant

amyloid-associated ^{11}C-PiB accumulation in the living brains, taking advantage of the high-quality ^{11}C-PiB with high specific radioactivity up to approximately 300 GBq/umol, 6-10 times higher than the usually used level, and very elderly mice (29 months). Our comparative analysis showed great consistency in the quantitative detection of Aβ deposition between ^{123}I-DRM106 and ^{11}C-PiB, demonstrating that SPECT imaging with ^{123}I-DRM106 has similar quantitativity and sensitivity as PET with ^{11}C-PiB in the living brain.

Based on our experimental result that the LTCx-to-CA1 ratio of binding of ^{125}I-DRM106 is significantly lower than that of ^{11}C-PiB, different pathological aggregates are expected to provide major binding sites for ^{125}I-DRM106 and ^{11}C-PiB. Although the LTCx-to-CA1 ratio of binding of ^{125}I-DRM106 was similar to that of ^{11}C-PBB3, which binds to both Aβ and tau aggregates at the incubation concentration used (*19*), NFTs might not provide binding sites for ^{125}I-DRM106, since a high concentration of non-radiolabeled DRM106 failed to fully block the binding of ^{11}C-PBB3 when we postulated that NFTs provide similar binding sites for all of the β-sheet ligands. Thus, a reasonable explanation is that ^{125}I-DRM106 might preferentially bind to dense-cored/neuritic plaques as did other amyloid tracers such as ^{18}F-FACT (*24*). Given that ^{11}C-PiB also binds to diffuse plaques, in addition to

dense-cored/neuritic plaques, the lower LTCx-to-CA1 ratio of binding of ^{125}I-DRM106 than ^{11}C-PiB is consistent with the distribution of Aβ plaques, that is, the major Aβ deposition is dense-cored/neuritic plaques in CA1. In contrast, in addition to dense-cored/neuritic plaques, numerous diffuse plaques are also observed in the LTCx region.

The correlation between PiB binding and the amounts of either Aβ(1-40) or Aβ(1-42) was not significant (*20*), being attributable to preferential binding of PiB to certain Aβ subtypes, such as $A\beta_{N3(pE)}$ (*2*). In contrast, ^{125}I-DRM106 binding showed excellent linearity with the amounts of either Aβ(1-40) or Aβ(1-42) in Tg2576 brain homogenates, suggesting that the terminal modification of Aβ may not change its binding sites for DRM106. If so, binding sites for DRM106 in AD patients and experimental animal models are more similar to each other compared to that for ^{11}C-PiB. As evidence, the ratio of B_{max} values of DRM106 for high-affinity binding sites in 20-month-old Tg2576 mouse to that in AD brain was proximately 0.17, very much higher than that of PiB (ratio of B_{max} values in 15-month-old APP/PS1 double-Tg mouse to AD brain was below 0.001) (*20*). Based on the binding potential (BP) values for high- and low-affinity binding sites in Tg2576 mouse brain being approximately 27 and 14, respectively, the percentage of BP for high-affinity binding is estimated as approximately 65%. Likewise, the percentage of BP for high-affinity binding

in AD brain is estimated as approximately 69% (Table 1). These two similar values may imply a similarity of composition of binding sites for DRM106 in Tg2576 and AD brains, largely differing from that seen in PiB binding to AD model mouse and patient brains (% of BP for high affinity binding was approximately 37% and 92% in AD model mouse and patient brains, respectively) (*20*). This suggests that $^{123/125}$I-DRM106 is more suitable than ^{11}C-PiB for translational research of the progression of amyloid pathology when using existing APP transgenic mouse models, most of which express numerous dense-cored, but not AD-like diffuse plaques.

CONCLUSION

In this study, we have successfully captured Aβ deposition in living AD model mouse with a newly developed SPECT agent, ^{123}I-DRM106. Given that its capacity was not inferior to ^{11}C-PiB for detecting Aβ deposition, ^{123}I-DRM106 has a high potential for further clinical application and, in fact, might preferentially capture the deposition of dense-cored/neuritic plaques.

DISCLOSURE

No potential conflict of interest relevant to this article was reported.

ACKNOWLEDGMENTS

The authors thank Prof. John Q. Trojanowski and Prof. Virginia M.-Y. Lee (Center for Neurodegenerative Disease Research, University of Pennsylvania) for kindly providing human tissue. This work was supported in part by Grants-in-Aid for Japan Advanced Molecular Imaging Program and Core Research for Evolutional Science and Technology (T. S.) and Scientific Research on Innovative Areas ("Brain Environment") 23111009 (M. H.) from the Ministry of Education, Culture, Sports, Science and Technology, Japan.

REFERENCES

1. Braak H, Braak E. Neuropathological staging of Alzheimer-related changes. *Acta Neuropathol (Berl).* 1991;82,239-259.
2. Maeda J, Ji B, Irie T, et al. Longitudinal, quantitative assessment of amyloid, neuroinflammation, and anti-amyloid treatment in a living mouse model of Alzheimer's disease enabled by positron emission tomography. *J Neurosci.* 2007;27,10957-10968.
3. Klunk WE, Engler H, Nordberg A, et al. Imaging brain amyloid in Alzheimer's disease with Pittsburgh Compound-B. *Ann Neurol.* 2004;55,306-319.
4. Engler H, Forsberg, A, Almkvist O, et al. Two-year follow-up of amyloid deposition in patients with Alzheimer's disease. *Brain.* 2006;129,2856-2866.
5. Ikonomovic MD, Klunk WE, Abrahamson EE, et al. Post-mortem correlates of in vivo PiB-PET amyloid imaging in a typical case of Alzheimer's disease. *Brain.* 2008;131,1630-1645.
6. Leinonen V, Alafuzoff I, Aalto S, et al. Assessment of β-amyloid in a frontal cortical brain biopsy specimen and by positron emission tomography with carbon 11-labeled Pittsburgh Compound B. *Arch Neurol.* 2008;65,1304-1309.
7. Okello A, Koivunen J, Edison P, et al. Conversion of amyloid positive and negative MCI to AD over 3 years: an ^{11}C-PIB PET study. *Neurology*. 2009;73,754-760.
8. Zhang W, Kung MP, Oya S, et al. 18F-labeled styrylpyridines as PET agents for amyloid plaque imaging. *Nucl Med Biol.* 2007;34,89-97.
9. Choi SR, Golding G, Zhuang Z, et al. Preclinical properties of ^{18}F-AV-45: a PET agent for Aβ plaques in the brain. *J Nucl Med.* 2009;50,1887-1894.
10. Hampel H, Wilcock G, Andrieu S, et al. Biomarkers for Alzheimer's disease therapeutic trials. *Prog Neurobiol.* 2011;95,579-593.
11. Cselenyi Z, Jonhagen ME, Forsberg A, et al. Clinical Validation of ^{18}F-AZD4694, an Amyloid-β-Specific PET Radioligand. *J Nucl Med.* 2012;53,415-424.
12. Kung MP, Hou C, Zhuang ZP, et al. Characterization of IMPY as a potential imaging agent for β-amyloid plaques in double transgenic PSAPP mice. *Eur J Nucl Med Mol Imaging.* 2004;31,1136-1145.
13. Kung MP, Hou C, Zhuang ZP, et al. IMPY: an improved thioflavin-T derivative for in vivo labeling of β-amyloid plaques. *Brain Res.* 2002;956,202-210.

14. Hsiao IT, Huang CC, Hsieh CJ, et al. Correlation of early-phase ^{18}F-florbetapir (AV-45/Amyvid) PET images to FDG images: preliminary studies. *Eur J Nucl Med Mol Imaging.* 2012;39,613-620.
15. Newberg AB, Wintering NA, Plossl K, et al. Safety, biodistribution, and dosimetry of ^{123}I-IMPY: a novel amyloid plaque-imaging agent for the diagnosis of Alzheimer's disease. *J Nucl Med.* 2006;47,748-754.
16. Song PJ, Bernard S, Sarradin P, et al. IMPY, a potential β-amyloid imaging probe for detection of prion deposits in scrapie-infected mice. *Nucl Med Biol.* 2008;35,197-201.
17. Kung MP, Weng CC, Lin KJ, et al. Amyloid plaque imaging from IMPY/SPECT to AV-45/PET. *Chang Gung Med J.* 2012;35,211-218.
18. Chen CJ, Bando K, Ashino H, et al. Synthesis and biological evaluation of novel radioiodinated imidazopyridine derivatives for amyloid-β imaging in Alzheimer's disease. *Bioorgan Med Chem.* 2014;22,4189-4197.
19. Maruyama M, Shimada H, Suhara T, et al. Imaging of tau pathology in a tauopathy mouse model and in Alzheimer patients compared to normal controls. *Neuron.* 2013;79,1094-1108.
20. Klunk WE, Lopresti BJ, Ikonomovic MD, et al. Binding of the positron emission tomography tracer Pittsburgh compound-B reflects the amount of amyloid-β in Alzheimer's disease brain but not in transgenic mouse brain. *J Neurosci.* 2005;25,10598-10606.
21. Ono M, Cheng Y, Kimura H, et al. Development of novel ^{123}I-Labeled pyridyl benzofuran derivatives for SPECT imaging of β-Amyloid plaques in Alzheimer's disease. *PLOS ONE.* 2013;8,e74104.
22. Kawarabayashi T, Younkin LH, Saido TC, et al. Age-dependent changes in brain, CSF, and plasma amyloid β protein in the Tg2576 transgenic mouse model of Alzheimer's disease. *J Neurosci.* 2001;21,372-381.
23. Snellman A, Rokka J, Lopez-Picon FR, et al. Pharmacokinetics of [^{18}F]flutemetamol in wild-type rodents and its binding to β amyloid deposits in a mouse model of Alzheimer's disease. *Eur J Nucl Med Mol Imaging.* 2012;39,1784-1795.
24. Ito H, Shinotoh H, Shimada H, et al. Imaging of amyloid deposition in human brain using positron emission tomography and [^{18}F]FACT: comparison with [^{11}C]PIB.

Eur J Nucl Med Mol Imaging. 2014;41,745-754.

FIGURES AND LEGENDS

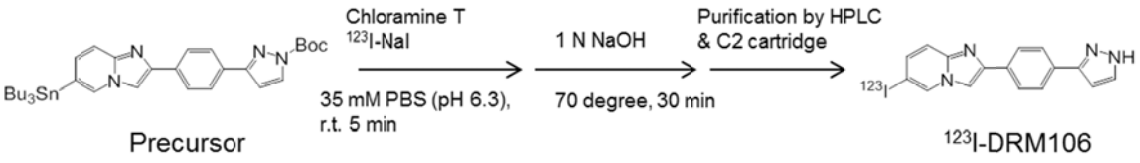

Fig. 1. Radiosynthesis for ^{123}I-DRM106

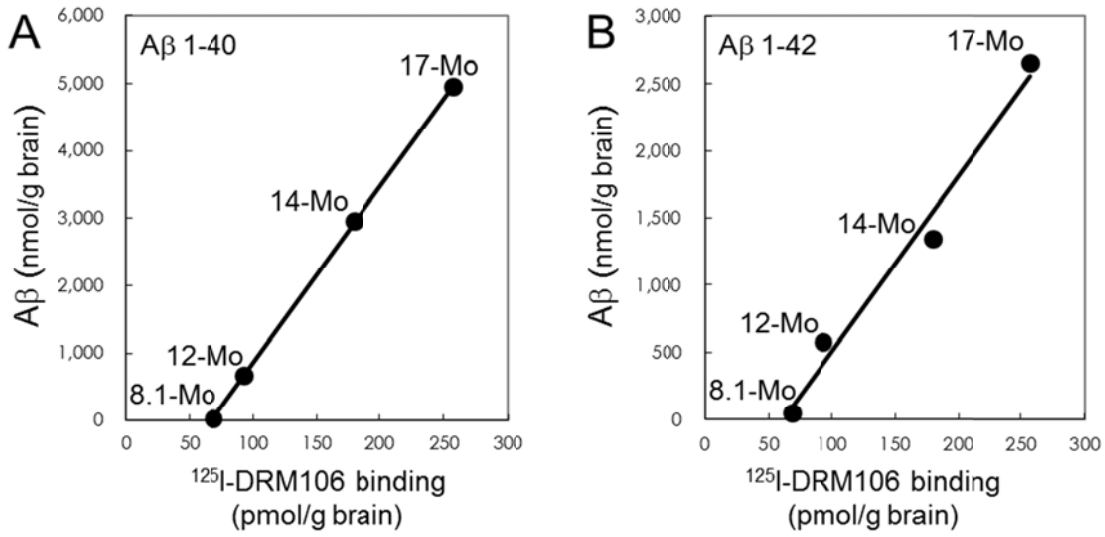

Fig. 2. Correlation between the amounts of Aβ species and binding of ^{125}I-DRM106. ^{125}I-DRM106 binding and the amounts of Aβ were increased age-dependently in brain homogenates of Tg mice at different ages as indicated, and the correlations between ^{125}I-DRM106 binding and Aβ(1-40) (A) and Aβ(1-42) (B) amounts were statistically significant. Data were from average of triplicate experiments for each age group. Mo, months

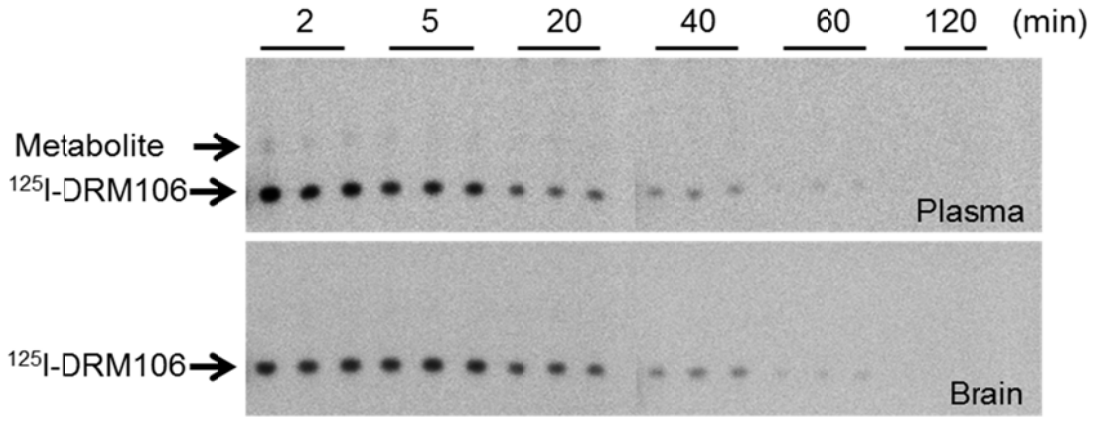

Fig. 3. Metabolic stability of DRM106 in Tg mice. The plasma and brain samples were collected at indicated time points after i.v. injection of ^{125}I-DRM106. Thin-layer chromatography (TLC) analysis clearly demonstrated that no overt metabolite in brain (lower panel) and only a little metabolite in plasma (upper panel) was detectable at the initial phase during the observation period.

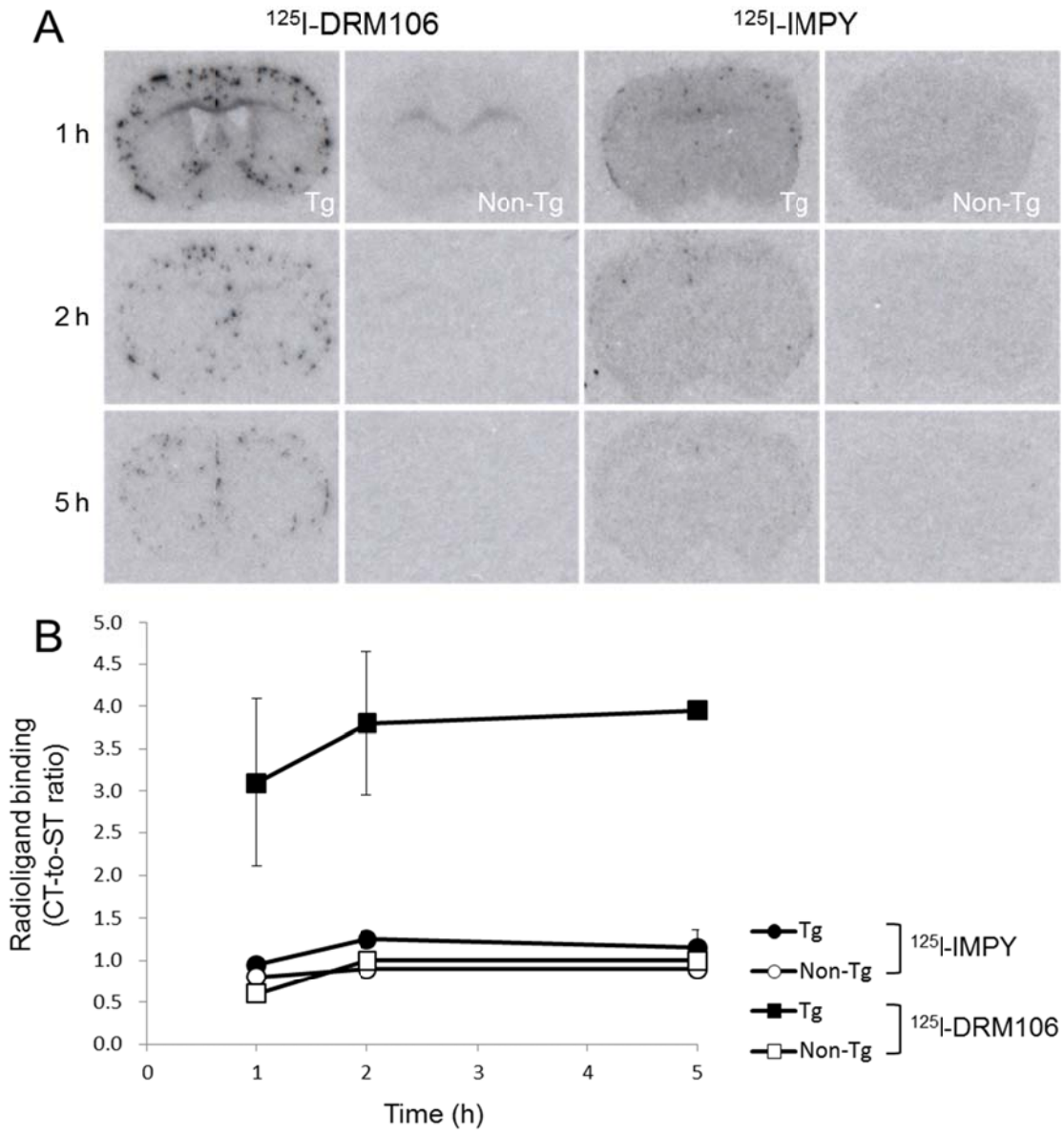

Fig. 4. Ex autoradiographic analysis of ^{125}I-DRM106 and ^{125}I-IMPY in Tg mouse brain. **A:** The representative coronal images of 18-month-old male Tg (from left, first and third columns) and body weight-matched non-Tg (from left, second and fourth columns) mice

having received bolus injection of radiolabeled ^{125}I-DRM106 (from left, first and second columns) and ^{125}I-IMPY (from left, third and fourth columns) at 1, 2 and 5 hours post-injection. **B:** Amyloidosis-associated accumulations of radioligands were quantified as ratios of radioactivity of neocortex (CT) to striatum (ST). Data were from experiments shown in Panel A. Tg (closed symbols, n = 2 for each time point) and non-Tg (open symbols, n = 1 for each time point) mice were administered with ^{125}I-DRM106 (squares) and ^{125}I-IMPY (circles). Data were expressed as mean ± SD.

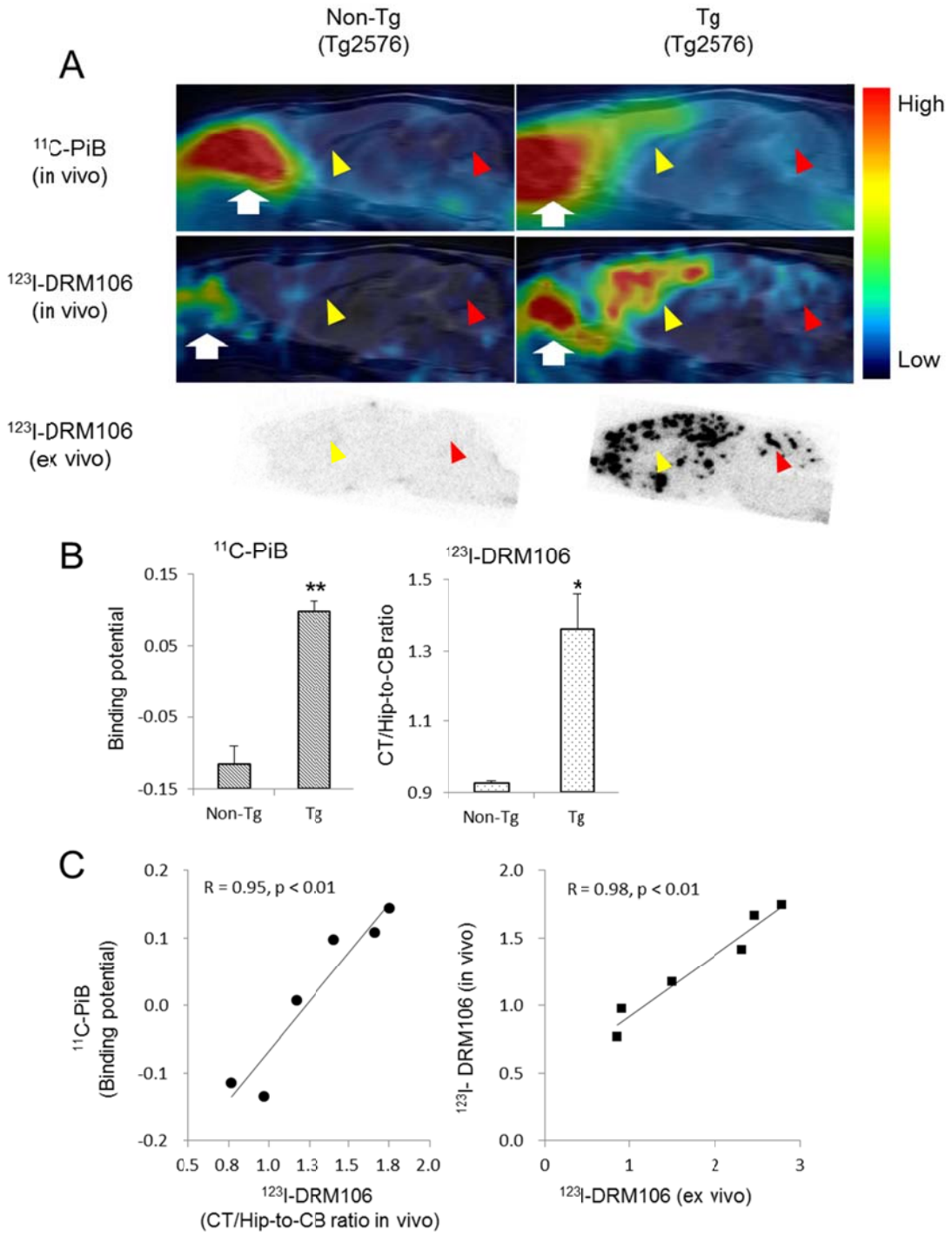
A
Non-Tg
(Tg2576)
Tg
(Tg2576)
11C-PiB
(in vivo)
123I-DRM106
(in vivo)
123I-DRM106
(ex vivo)
High
Low
B
11C-PiB
Binding potential
0.15
0.05
-0.05
-0.15
**
Non-Tg
Tg
123I-DRM106
CT/Hip-to-CB ratio
1.5
1.3
1.1
0.9
*
Non-Tg
Tg
C
R = 0.95, p < 0.01
11C-PiB
(Binding potential)
0.2
0.1
0.0
-0.1
-0.2
0.5 0.8 1.0 1.3 1.5 1.8 2.0
123I-DRM106
(CT/Hip-to-CB ratio in vivo)
R = 0.98, p < 0.01
123I- DRM106 (in vivo)
2.0
1.5
1.0
0.5
0.0
0 1 2 3
123I-DRM106 (ex vivo)

Fig. 5. In vivo imaging with ^{123}I-DRM106 and ^{11}C-PiB. **A:** Top, middle and bottom panels illustrate typical in vivo images of ^{11}C-PiB and ^{123}I-DRM106, and ex vivo images of ^{123}I-DRM106, respectively, in a 28-month-old female Tg (Tg2576; right column) and an age-matched non-Tg littermate (left column) mouse brains, and in vivo images were overlaid on the MRI template. Red and yellow arrowheads indicate CB and CT/Hip regions. White arrows indicate harderian gland. **B:** Quantitative analysis for in vivo binding of ^{11}C-PiB and ^{123}I-DRM106 in non-Tg (n = 3) and Tg (n = 5) mice. In vivo bindings of ^{11}C-PiB and ^{123}I-DRM106 were estimated by binding potential and CT-to-CB ratio, respectively. Data were expressed as mean ± SD. *, $p<0.05$, **, $p<0.01$, vs non-Tg mouse, t-test. **C:** Correlation of in vivo binding between ^{11}C-PiB and ^{123}I-DRM106 (left), and between in vivo and ex vivo binding of ^{123}I-DRM106 (right). The data of those mouse individuals, which received both ^{11}C-PiB and ^{123}I-DRM106 scans, were used for correlation analysis.

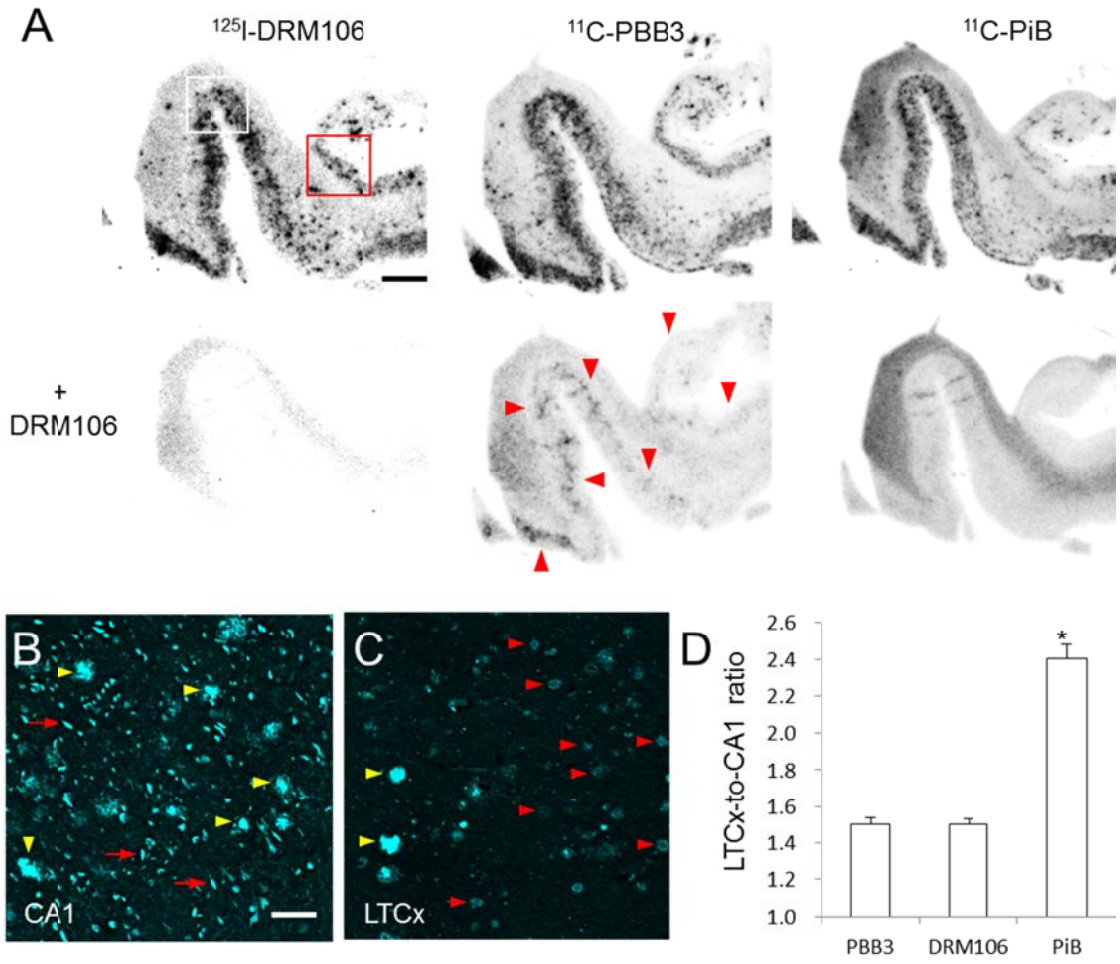

Fig. 6. In vitro autoradiographic analyses with ^{125}I-DRM106, ^{11}C-PiB, and ^{11}C-PBB3 in postmortem AD brains. **A**: Autoradiographic images of ^{125}I-DRM106 (left), ^{11}C-PBB3 (middle) and ^{11}C-PiB (right), and in the absence (upper panel) or presence (lower panel) of non-radiolabeled DRM106 in brain sections from a patient with AD. The slices contain hippocampus, parahippocampal gyrus, and fusiform gyrus. The areas outlined with white

and red squares contain hippocampal CA1 and lateral temporal cortex (LTCx) flanking the collateral sulcus, respectively, and high-power images of these two regions are shown in ***Supplementary Information*** (SFig. 4). Red arrowheads indicate putative NFT-associated binding of ^{11}C-PBB3. **B, C:** Fluorescent counterstaining of NFTs (red arrows), dense-cored/neuritic (yellow arrowheads) and diffuse (red arrowheads) plaques with FSB in CA1 (B) and LTCx (C) regions. **D**: Serial brain sections (5, 4 and 4 randomized sections for analyses of ^{125}I-DRM106, ^{11}C-PiB and ^{11}C-PBB3, respectively) from a patient with AD were used for quantitative analyses of specific bindings of these radiolabeled ligands. There was significant main effect ($F_{(2, 10)} = 6.32$, $p < 0.05$ by one-way ANOVA). *Post hoc* analysis revealed that the LTCx-to-CA1 ratio of ^{11}C-PiB was significantly higher as compared to those of ^{125}I-DRM106 and ^{11}C-PBB3 (*, $p < 0.05$, Bonferroni). Data were expressed as mean ± SD. Scale bars: A, 5 mm; B, C, 50 μm.

TABLES

Table 1. Binding parameters of ^{125}I-DRM106

Sample	High affinity binding site			Low affinity binding site		
	K_d[a]	B_{max}[b]	BP[c]	K_d	B_{max}	BP
Aβ1-40 fibrils (n=4)	1.50 ± 0.00	4.30 ± 1.00	-	1400 ± 36.6	163 ± 9.60	-
Aβ1-42 fibrils (n=4)	10.1± 5.10	34.3 ± 22.8	-	2890 ± 344.5	339 ± 268	-
Tg brain (n=4)	4.20 ± 0.92	113 ± 133	26.9	264 ± 160	3780 ± 1008	14.3
AD brain	4.30 ± 1.20	681 ± 305	158.4	101 ± 37.8	7050 ± 1985	69.8

[a], K_d was expressed as nmol/L.

[b], B_{max} for Aβ fibrils and mouse/human tissues were expressed as pmol/nmol of Aβ and pmol/g tissue.

[c], Binding potential (BP) = B_{max} / K_d

Data of Aβ fibrils were from 4 independent experiments, and each experiment was run in triplicate.

Data of Tg brains were from 4 mice (20 months old), and each experiment was run in triplicate.

Data of AD brain were from triplicate experiments.

Data were expressed as mean ± SD.